Higher-Order Spike Triggered Analysis of Neural Oscillators

Keisuke Ota[1], Toshiaki Omori[2], Hiroyoshi Miyakawa[3], Masato Okada[1,4], Toru Aonishi[5]*

1 Brain Science Institute, RIKEN, Wako-shi, Saitama, Japan, 2 Department of Electrical and Electronic Engineering, Kobe University, Kobe-shi, Hyogo, Japan, 3 School of Life Sciences, Tokyo University of Pharmacy and Life Sciences, Hachioji, Tokyo, Japan, 4 Department of Complexity Science and Engineering, The University of Tokyo, Kashiwa-shi, Chiba, Japan, 5 Department of Computational Intelligence and Systems Science, Tokyo Institute of Technology, Yokohama-shi, Kanagawa, Japan

Abstract

For the purpose of elucidating the neural coding process based on the neural excitability mechanism, researchers have recently investigated the relationship between neural dynamics and the spike triggered stimulus ensemble (STE). Ermentrout et al. analytically derived the relational equation between the phase response curve (PRC) and the spike triggered average (STA). The STA is the first cumulant of the STE. However, in order to understand the neural function as the encoder more explicitly, it is necessary to elucidate the relationship between the PRC and higher-order cumulants of the STE. In this paper, we give a general formulation to relate the PRC and the nth moment of the STE. By using this formulation, we derive a relational equation between the PRC and the spike triggered covariance (STC), which is the covariance of the STE. We show the effectiveness of the relational equation through numerical simulations and use the equation to identify the feature space of the rat hippocampal CA1 pyramidal neurons from their PRCs. Our result suggests that the hippocampal CA1 pyramidal neurons oscillating in the theta frequency range are commonly sensitive to inputs composed of theta and gamma frequency components.

Introduction

A neural system can be considered to be an encoder which transforms specific external stimuli into neural spikes. One of the main goals of neuroscience is to identify the stimuli from the observed spikes. Spike triggered analysis is a powerful way to achieve this goal. In this analysis, we give stochastic stimuli to a neural system and identify the set of stimuli that induce the neurons to spike [1]. This set is called the spike triggered stimulus ensemble (STE) [2–4]. For example, the linear receptive field components in V1 simple cells can be discerned from the spike triggered average (STA), which is the average of STE [5,6]. Additionally, the spike triggered covariance (STC) which is the covariance of the STE helps to clarify the receptive field structure of complex cells representing the nonlinear response [7,8].

The traditional spike-triggered analysis with sensory stimuli can extract the receptive field properties of sensory neurons. Using direct current injection stimuli instead of sensory stimuli, the spike-triggered analysis can extract the set of presynaptic inputs encoded by individual neurons. The big advantage of the spike-triggered analysis with direct current injection stimuli is that it enables us to capture the coding properties of neurons in higher brain regions, such as the hippocampal regions, which are far away from the lower order sensory regions.

This spike triggered analysis can be formulated in terms of Bayes' rule,

$$P[\xi(\tau < t_s)|\, spike\ at\ t_s] \propto P[spike\ at\ t_s|\xi(\tau < t_s)]\, P[\xi(\tau < t_s)], \quad (1)$$

where t_s is spike time and $\xi(\tau < t_s)$ is a stimulus which has been applied to neurons before t_s. $P[\xi(\tau < t_s)|\, spike\ at\ t_s]$ is the probability density function (PDF) of the STE; it is the conditional PDF of the stimulus $\xi(\tau < t_s)$ given the spike timing t_s. $P[spike\ at\ t_s|\xi(\tau < t_s)]$ represents the spike generation process of the neural systems and is the PDF of the spike timing t_s given the stimulus $\xi(\tau < t_s)$, and $P[\xi(\tau < t_s)]$ is the PDF of the stochastic stimulus applied to the neural systems. The PDF of the STE or statistics can be identified in two ways. One is the indirect way, in which $P[spike\ at\ t_s|\xi(\tau < t_s)]$ is determined and then $P[\xi(\tau < t_s)|\, spike\ at\ t_s]$ is obtained from Eq. (1). The other way is to obtain the distribution directly by measuring spike timings of neural systems in response to the stochastic stimulus $P[\xi(\tau < t_s)]$. The direct way is almost always used for the spike triggered analysis in vivo experiments.

To clarify the relationship between neural dynamics and neural coding, several groups have recently tried to identify the STE statistics (i.e. STA and STC) in the indirect way [9–12]. Ermentrout et al. related neural dynamics to neural coding when regularly firing neurons are disturbed by sufficiently small white noise [13]. They analytically proved that the STA is proportional to the temporal differentiation of phase response curve (PRC), which represents an impulse response of an oscillatory system and

captures the essence of the neural dynamics. Furthermore, they performed whole cell recording from olfactory bulb mitral cells and showed that their theory holds true for real cells. They made progress in relating the neural dynamics to the neural coding for real oscillating neurons. However, the STA is the first cumulant of the STE. To better understand the neural encoder function, it will be necessary to elucidate the relationship between the PRC and the higher-order moments of the STE.

In this paper, we focus on the neurons spiking almost periodically on the same assumption as Ermentrout et al. We propose a general formulation to relate the PRC and the nth moment of the STE ($MSTE_n$) based on the Bayes' rule in Eq. (1) [14]. In fact, we derive two relational equations. One relates the PRC to the STA, and the other relates the PRC to the STC. The relational equation between the STA and PRC coincides with the equation derived in [13]. This consistency shows that our formulation method includes Ermentrout et al.'s framework and is an extension of their theory. Additionally, the relational equation between the PRC and the STC allows us to determine the feature space, which is a low-dimensional subspace of the full stimulus space and characterizes the stimulus encoded by neurons [3,10,11]. We apply the relational equation to identifying the feature space of hippocampal CA1 pyramidal neurons oscillating in the theta frequency range (4–14 Hz) [15–17] from the estimated PRCs [18]. We show that the first principal component representing the feature space is the suppressive eigenfunction mainly composed of theta frequency components, whereas the second principal component is the excitatory eigenfunction mainly composed of gamma frequency components [19,20].

Methods

Phase Description of Spike Generation Process

We will begin by describing the spike generation process of the oscillating neurons. Let us consider regularly firing neurons perturbed by sufficiently small white Gaussian noise stimulus. This neural behavior can be described by

$$\frac{d\mathbf{X}}{dt} = F(\mathbf{X}) + \sigma\xi(t), \tag{2}$$

where $\mathbf{X}$ is the state of the neuron, $F(\mathbf{X})$ the vector field of neural dynamics, $\xi(t)$ the white Gaussian noise stimulus, and σ the stimulus intensity. $d\mathbf{X}/dt = F(\mathbf{X})$ has a stable limit cycle solution $\mathbf{X}_0(t)$ with period T. When the stimulus intensity is sufficiently small ($\sigma \ll 1$), we can apply the phase reduction method [21] to Eq. (2) and obtain the following Langevin phase equation (LPE) [18,22–25]:

$$\frac{d\phi}{dt} = 1 + \sigma Z(\phi) \cdot \xi(t). \tag{3}$$

Here, $\phi(t)$ represents the phase defined along the limit cycle solution $\mathbf{X}_0(t)$ and $Z(\phi)$ represents the PRC that corresponds to the impulse response function quantifying the phase response of the neural oscillator to the small perturbations. By introducing a slow phase variable $\psi(t)$ as $\phi(t) = t + \psi(t)$, Eq. (3) can be transformed into

$$\frac{d\psi}{dt} = \sigma Z(t+\psi) \cdot \xi(t). \tag{4}$$

Let t_s be the spike time after the first spike at $t=0$. Since $\phi(t_s) = T$,

t_s is given by

$$t_s = T - \psi(t_s). \tag{5}$$

By integrating both sides of Eq. (4) from $t=0$ to $t=t_s$, we can describe $\psi(t_s)$ in terms of the PRC as follows:

$$\psi(t_s) = \sigma \int_0^{t_s} dt\, Z(t+\psi(t)) \cdot \xi(t), \tag{6}$$

where $\psi(0) = 0$. Since ψ varies slowly when $\sigma \ll 1$, we can expand the right-hand side of Eq. (6) [23,26]:

$$
\begin{aligned}
\psi(t_s) &= \sigma \int_0^{t_s} dt_1\, Z(t_1)\xi(t_1) \\
&\quad + \sigma^2 \int_0^{t_s} dt_1 \int_0^{t_1} dt_2\, Z'(t_1)Z(t_2)\xi(t_1)\xi(t_2) + \cdots \\
&= \sigma\psi_1(t_s) + \sigma^2\psi_2(t_s) + \cdots.
\end{aligned}
\tag{7}
$$

This is now in the form of a Volterra series, which is widely used in analyzing oscillators driven by noise. Here, $\psi_1(t)$ corresponds to a linear convolution term, which is derived under the assumption that ψ stops during a change of $\xi(t)$. $\psi_2(t_s)$ corresponds to the noise-induced drift in the Stratonovich definition [27]. It stems from the fact that $\psi(t)$ also changes when $\xi(t)$ changes.

General Formulation for the nth Moment of STE

Next, let us describe the nth moment of STE ($MSTE_n$). $MSTE_n$ is defined as the nth time correlation of the current input $\sigma\xi(t_s - \tau_i)$, which represents the input preceding the spike time t_s by $\tau_i (i=1,2,\cdots,n)$. On the basis of Hong et al.'s formulation [14], $MSTE_n$ for the neural oscillators can be described with Bayes' rule in Eq. (1):

$$
\begin{aligned}
&MSTE_n(\tau_1,\cdots,\tau_n) = \\
&\left\langle \sigma^n \int_{-\infty}^{\infty} dt_s\, \delta(t_s - T + \psi(t_s)) \prod_{i=1}^n \xi(t_s - \tau_i) \right\rangle_\xi,
\end{aligned}
\tag{8}
$$

where $\delta(t_s - T + \psi(t_s))$ is the probability density of spike timings corresponding to $P[\text{spike at } t_s | \xi(\tau < t_s)]$ in Eq. (1) and $\langle\ \rangle_\xi$ represents $\int d\xi(\tau < t_s) P[\xi(\tau < t_s)]$. Because Eq. (8) represents integrals of the probability density of Eq. (1) over all stimulus inputs and all spike times t_s, this equation gives $MSTE_n$ as the expected value of $\prod_{i=1}^n \xi(t_s - \tau_i)$ integrated over all spike times t_s.

Here, we shall denote the m-th order derivative of the delta function as $\delta^{(m)}(x)$, and write the Taylor expansion of the delta function as $\delta(x + \Delta x) = \sum_{m=0}^{\infty} \delta^{(m)}(x)(\Delta x)^m / m!$ ($\Delta x \ll 1$), where $\delta^{(0)}(x) = \delta(x)$ and $0! = 1$. Since $\sigma \ll 1$, the right-hand side of Eq. (8) can be expanded as follows:

$$
\begin{aligned}
&MSTE_n(\tau_1,\cdots,\tau_n) = \\
&\left\langle \sigma^n \int_{-\infty}^{\infty} dt_s \sum_{m=0}^{\infty} \frac{\delta^{(m)}(t_s - T)}{m!} \psi(t_s)^m \prod_{i=1}^n \xi(t_s - \tau_i) \right\rangle_\xi.
\end{aligned}
\tag{9}
$$

This is the relational equation between the $MSTE_n$ and the PRC, because $\psi(t_s)$ is represented by the PRC in Eq. (7).

Relating STA and STC to the PRC

We can analytically derive the STA or the STC from Eq. (9) when $\xi(t)$ is zero-mean Gaussian white noise. In this case, higher correlation functions are given by $\langle \xi(t_1)\xi(t_2)\cdots\xi(t_{2n-1})\rangle_\xi = 0$ and $\langle \xi(t_1)\xi(t_2)\cdots\xi(t_{2n})\rangle_\xi = \sum \delta(t_{i_1}-t_{i_2})\delta(t_{i_3}-t_{i_4})\cdots\delta(t_{i_{2n-1}}-t_{i_{2n}})$. Here, the sum has to be performed over those $(2n)!/2^n n!$ permutations in which $2n$ elements are separated into n pairs [27]. The correlation of the raw stimulus input is

$$C_{\text{raw}}(\tau_1,\tau_2) = \langle \sigma^2 \xi(t_s-\tau_1)\xi(t_s-\tau_2)\rangle_\xi = \sigma^2 \delta(\tau_1-\tau_2) \quad (10)$$

We shall first derive an approximate equation relating the STA to the PRC. The STA is defined as the first moment of the STE: $STA(\tau_1) = MSTE_1(\tau_1)$. Substituting Eq. (7) into Eq. (9) and evaluating the lowest order, we obtain the approximated equation relating the STA to the PRC as

$$
\begin{aligned}
STA(\tau_1) &= MSTE_1(\tau_1) \\
&\approx \left\langle \sigma^2 \int_{-\infty}^{\infty} dt_s \delta^{(1)}(t_s-T)\psi_1(t_s)\xi(t_s-\tau_1)\right\rangle_\xi \\
&= \sigma^2 \int_{-\infty}^{\infty} dt_s \int_0^{t_s} dt_1 \delta^{(1)}(t_s-T)Z(t_1)<\xi(t_1)\xi(t_s-\tau_1)>_\xi \\
&= \sigma^2 \int_{-\infty}^{\infty} dt_s \int_0^{t_s} dt_1 \delta^{(1)}(t_s-T)Z(t_1)\delta(t_1-t_s+\tau_1) \\
&= \sigma^2 \int_{-\infty}^{\infty} dt_s \delta^{(1)}(t_s-T)Z(t_s-\tau_1). \\
&= -\sigma^2 Z'(T-\tau_1).
\end{aligned}
\tag{11}
$$

To obtain the last line, we used the delta function property, $\int_{-\infty}^{\infty} \delta^{(n)}(x-a)f(x)dx = (-1)^n f^{(n)}(a)$. This result is consistent with the equation derived by Ermentrout et al. [13].

Next, we derive the approximated equation relating the STC to the PRC. The STC is defined as the second moment around the STA: $STC(\tau_1,\tau_2) = MSTE_2(\tau_1,\tau_2) - STA(\tau_1)\cdot STA(\tau_2)$. Similarly, substituting Eq. (7) into Eq. (9) and evaluating the $O(\sigma^2)$ and $O(\sigma^4)$, we obtain

$$
\begin{aligned}
MSTE_2(\tau_1,\tau_2) &\approx \left\langle \sigma^2 \int_{-\infty}^{\infty} dt_s \delta(t_s-T)\xi(t_s-\tau_1)\xi(t_s-\tau_2)\right\rangle_\xi \\
&+ <\sigma^4 \int_{-\infty}^{\infty} dt_s \delta^{(1)}(t_s-T)\psi_2(t_s)\xi(t_s-\tau_1)\xi(t_s-\tau_2)>_\xi \\
&+ <\frac{\sigma^4}{2}\int_{-\infty}^{\infty} dt_s \delta^{(2)}(t_s-T)\psi_1(t_s)^2\xi(t_s-\tau_1)\xi(t_s-\tau_2)>_\xi.
\end{aligned}
\tag{12}
$$

Note that the $O(\sigma^2)$ term of $MSTE_2$ is equivalent to the variance of the raw stimulus ensemble C_{raw} and the $O(\sigma^3)$ term disappears since $\langle \xi(t_1)\xi(t_2)\xi(t_3)\rangle_\xi = 0$; therefore, we should evaluate $O(\sigma^4)$ term including the fourth order correlation $\langle \xi(t_1)\xi(t_2)\xi(t_3)\xi(t_4)\rangle_\xi$. The second term in the right-hand side of Eq. (12) is

$$
\begin{aligned}
&\left\langle \sigma^4 \int_{-\infty}^{\infty} dt_s \delta^{(1)}(t_s-T)\psi_2(t_s)\xi(t_s-\tau_1)\xi(t_s-\tau_2)\right\rangle_\xi \\
&= \sigma^4 \int_{-\infty}^{\infty} dt_s \int_0^{t_s} dt_1 \int_0^{t_1} dt_2 \delta^{(1)}(t_s-T)Z'(t_1)Z(t_2) \\
&\quad \times (\delta^{(1)}(t_1-t_s+\tau_1)\delta(t_2-t_s+\tau_2) \\
&\quad + \delta^{(1)}(t_1-t_s+\tau_2)\delta(t_2-t_s+\tau_1) + \delta^{(1)}(t_1-t_2)\delta(\tau_1-\tau_2)),
\end{aligned}
\tag{13}
$$

and the third term is

$$
\begin{aligned}
&\left\langle \frac{\sigma^4}{2}\int_{-\infty}^{\infty} dt_s \delta^{(2)}(t_s-T)\psi_1(t_s)^2\xi(t_s-\tau_1)\xi(t_s-\tau_2)\right\rangle_\xi \\
&= \frac{\sigma^4}{2}\int_{-\infty}^{\infty} dt_s \int_0^{t_s} dt_1 \int_0^{t_s} dt_2 \delta^{(2)}(t_s-T)Z(t_1)Z(t_2) \\
&\quad \times (2\delta(t_1-t_s+\tau_1)\delta(t_2-t_s+\tau_2) + \delta(t_1-t_2)\delta(\tau_1-\tau_2)).
\end{aligned}
\tag{14}
$$

By using the delta function property again, we finally obtain the approximate equation relating the STC to the PRC as follows:

$$
\begin{aligned}
STC(\tau_1,\tau_2) &= \sigma^2 \delta(\tau_1-\tau_2) + \frac{1}{2}\sigma^4 Z'(T)Z(T)\delta(\tau_1-\tau_2) \\
&+ \sigma^4 H_{1/2}(\tau_2-\tau_1)Z''(T-\tau_2)Z(T-\tau_1) \\
&+ \sigma^4 H_{1/2}(\tau_1-\tau_2)Z''(T-\tau_1)Z(T-\tau_2),
\end{aligned}
\tag{15}
$$

where $H_{1/2}(x)$ represents a Heaviside function which takes $1/2$ at $x=0$.

Feature Space Extraction

Although the input stimulus space is of high dimensionality, the feature space, which is spanned by the stimuli encoded by neurons, is a low-dimensional subspace of the full stimulus space. The feature space can be extracted by conducting an eigenvalue analysis of the difference between the STC and the correlation of the raw stimulus input:

$$\Delta C(\tau_1,\tau_2) = STC(\tau_1,\tau_2) - C_{\text{raw}}(\tau_1,\tau_2) \tag{16}$$

The matrix of the STC represents the variance of a collection of samples in all possible directions within the space of spike-triggered stimuli, and ΔC captures the relative change of the variance of the ensemble of input stimuli due to the rearrangement of stimuli in the time window preceding each spike. The eigenvalue of ΔC, which is equal to the relative change of the variance in the direction of the corresponding eigenfuction, characterizes the sensitivity of neuron in response to the corresponding eigenfuction. The eigenfunctions with positive eigenvalues are referred to as the excitatory eigenfunctions, which enhance neural activity, whereas those with negative eigenvalues are called the suppressive eigenfunctions, which suppress neural activity. In the case of neural oscillators analyzed here, the stimuli in the subspace spanned by excitatory eigenfunctions cause shorter interspike intervals (ISIs) than the average period T, while the stimuli in the subspace spanned by suppressive eigenfunctions cause longer ISIs. Here, as in previous studies on spike triggered analyses for neural oscillators [28], we extract the feature space of

neurons by computing the set of eigenfunctions with the large nonzero eigenvalues of ΔC in absolute value.

PRCs of Hippocampal CA1 Pyramidal Neurons

We used PRCs obtained from hippocampal CA1 pyramidal neurons by performing whole-cell patch-clamp recordings in vitro in our previous work [18]. In our protocol for measuring PRCs, we inject DC depolarizing currents into somata of CA1 pyramidal neurons to evoke periodic firing. Using the dynamic clamp, the mean ISI is adjusted to the target period of T by tuning the DC depolarizing current. Next, a one-shot rectangle perturbation superimposed on the DC depolarizing current is evoked using various timings relative to the spike, and we measure how the perturbation current disturbs the timing of the succeeding spike. Spike times are randomly fluctuated by intrinsic noise in neurons. To extract PRCs from stochastic data of phase responses, we apply the maximum a posteriori (MAP) estimation algorithm that we proposed [29,30] to the in vitro data. As described in the Numerical experiments section of the Methods, the notable feature of this algorithm is its use of a detailed PRC measurement model formulated as an LPE, which is the same as the one used in the current study. The effectiveness of the measurement model and the reliability of the estimated PRCs were verified by testing whether the LPEs with the estimated PRCs could predict the stochastic behaviors of the same neurons, whose PRCs had been measured, when they were perturbed by various periodic stimulus currents. Detailed explanations of experimental conditions and the MAP estimation algorithm can be found in [29–31].

Numerical Experiments

Conductance-based model. To verify the algorithms by using numerical simulations, we use the Morris-Lecar (ML) model [32] in the form of

$$C\frac{dV}{dt} = -g_{Ca}m_\infty(V - V_{Ca}) - g_K w(V - V_K) \\ - g_{leak}(V - V_{leak}) + I_{ext},$$

(17)

where each ion channel has the following activation profile:

$$\frac{dw}{dt} = \phi \cdot \frac{w_\infty - w}{\tau},$$
$$m_\infty = 0.5[1 + \tanh((V - v_1)/v_2)],$$
$$w_\infty = 0.5[1 + \tanh((V - v_3)/v_4)],$$
$$\tau = 1/\cosh((V - v_3)/(2 \cdot v_4)).$$

Depending on the parameters, the ML model has different bifurcation structures, classified as Type I and Type II [32]. In Type I model, oscillations emerge through a saddle-node bifurcation on an invariant circle. The parameters for the Type I model used in the simulations are $C = 20\ \mu F$, $V_K = -84\ mV$, $g_K = 8\ mS$, $V_{Ca} = 120\ mV$, $g_{Ca} = 4\ mS$, $V_{leak} = -60\ mV$, $g_{leak} = 2\ mS$, $v_1 = -1.2\ mV$, $v_2 = 18\ mV$, $v_3 = 12\ mV$, $v_4 = 17.4\ mV$ and $\phi = 0.066$. In the Type II model, oscillations emerge through a Hopf bifurcation. The parameters for the Type II model used in the simulations are $C = 20\ mF$, $V_K = -84\ mV$, $g_K = 8\ mS$, $V_{Ca} = 120\ mV$, $g_{Ca} = 4.4\ mS$, $V_{leak} = -60\ mV$, $g_{leak} = 2\ mS$, $v_1 = -1.2\ mV$, $v_2 = 18\ mV$, $v_3 = 2\ mV$, $v_4 = 30\ mV$ and $\phi = 0.04$.

The extra current I_{ext} used in each numerical experiment is defined as follows.

Numerical calculation of STA and STC. By employing the Euler method, we numerically solved the ML model with the extra current I_{ext} in the form of

$$I_{ext} = I_c + \sigma\xi(t),$$

where I_c is the depolarizing constant current for inducing rhythmical firing with an average period T. $\xi(t)$ is the white Gaussian noise stimulus satisfying $<\xi(t)> = 0$ and $<\xi(t)\xi(t')> = 2\delta(t - t')$. σ is the intensity of the stimulus used in the numerical simulations. In the Type I model, $I_c = 41\ \mu A$ for $T = 195.83$ msec and $\sigma = 1.0\ \mu A$. In the Type II model, $I_c = 95\ \mu A$ for $T = 91.17$ msec and $\sigma = 6.0\ \mu A$.

In the numerical simulation, we measured the spike time, t_s while we stored the noise stimulus $\xi(t)$. Here, we denote the time of the ith spike as t_{si}, and the time sequence of the noise stimulus that were presented over an averaging interval T preceding the ith spike as $\xi(t_{si} - \tau)$, $(0 < \tau < T)$.

We numerically calculated the first moment of STE, $\mathrm{M}STE_1$ by taking the sample average of the stimuli [3,8]:

$$\mathrm{M}STE_1(\tau) = \frac{1}{N_s}\sum_{i=1}^{N_s}\xi(t_{si} - \tau),$$

where N_s indicates the number of samples. As described above, the first moment of STE is called the STA. In a similar fashion, we numerically obtained the second moment of STE, $\mathrm{M}STE_2$ by calculating the covariance of the stimuli [3,8]:

$$\mathrm{M}STE_2(\tau_1, \tau_2) = \frac{1}{N_s}\sum_{i=1}^{N_s}\xi(t_{si} - \tau_1)\xi(t_{si} - \tau_2).$$

Then, according to the definition of the STC [3,8], we can obtain the sample STC from the first and second moments:

$$STC(\tau_1, \tau_2) = \mathrm{M}STE_2(\tau_1, \tau_2) - \mathrm{M}STE_1(\tau_1)\mathrm{M}STE_1(\tau_2).$$

Adjoint method for calculating infinitesimal PRCs. We numerically calculated the infinitesimal PRCs of the ML model by using the adjoint method [21,33]. In this numerical calculation, we used the extra current in the form of $I_{ext} = I_c$ (i.e., without noise). In the same manner as above, I_c is the depolarizing constant current for inducing rhythmical firing with the period T. In the Type I model, $I_c = 41\ \mu A$ for $T = 195.83$ msec, and in the Type II model, $I_c = 95\ \mu A$ for $T = 91.17$ msec.

Generally, the adjoint to the linearization of the unperturbed oscillator, $dX/dt = F(X)$ in Eq. (2) on a limit cycle orbit $\Phi(t)$ satisfies:

$$\frac{dZ}{dt} = -JF(\Phi(t))^T Z(t),$$

where $JF(\Phi(t))^T$ is the transpose of the Jacobi matrix of F on the orbit. Due to the stability of the system in the orbit, the Jacobi matrix $JF(\Phi(t))$ only has nonpositive eigenvalues. Hence, the above adjoint system is unstable, and it has an unstable limit cycle orbit. This unstable limit cycle orbit corresponds to the

infinitesimal PRCs. By reversing the time in the numerical calculation, we can stably obtain the unstable limit cycle orbit.

Estimation of PRCs from artificial data. To check the applicability of the theory to real neurons, we used a PRC estimated from a finite sample of artificial phase responses generated with the Type I ML model. In the numerical simulation for generating artificial phase response data, we used an extra current I_{ext} in the form of

$$I_{ext} = I_c + G_p(t - t_0) + \gamma n(t),$$

where I_c is the depolarizing constant current for inducing rhythmical firing with an average period T, and $G_p(t - t_0)$ is the rectangle pulse current whose t_0 represents the timing of its appearance. $n(t)$ is white Gaussian noise satisfying $<n(t)> = 0$ and $<n(t)n(t')> = 2\delta(t - t')$, and γ is the intensity of the noise. The parameters we used are $I_c = 41\ \mu A$ for $T = 195.83$ msec, $\gamma = 0.45\ \mu A$, amplitude of $G_p = 20\ \mu A$, and duration of $G_p = 1.0$ msec.

By employing the Euler method, the phase response were sampled as a sequence of equidistant points, $t_0 = \Delta t j (j = 0, \cdots, L - 1)$, whose sampling period was $\Delta t = T/L$, and N samples of phase responses were measured at each sampling point $t_0 = \Delta t j$. Thus, the total number of data was LN. In the numerical experiment of this paper, $L = 20$ and $N = 10$.

We used the maximum a posteriori (MAP) estimation algorithm that we proposed in our previous papers to estimate the PRCs from the artificial data. The notable feature of this algorithm is its use of a detailed PRC measurement model formulated as the LPE, which is the same as the one used in this work. Moreover, our algorithm enables one to estimate hyperparameters including the

smoothness of the PRCs, whereas in previous studies, the smoothness was selected in an ad-hoc way. A detailed explanation of the MAP estimation algorithm can be found in [29,30].

Results

Simulation

In order to confirm our theory, we compared the STC calculated from Eq. (15) and the STC obtained in a numerical experiment. Figure 1 (A1) and (B1) show the numerically simulated STCs for Type I and Type II Morris-Lecar (ML) model [32], respectively. Figure 1 (A2) and (B2) illustrate the analytically derived STCs, where the PRCs for each ML model are derived with the adjoint method [21,33]. These analytically derived STCs are in good agreement with the numerically simulated ones. This result indicates that the STC can be computed accurately with our theory.

We conducted an eigenvalue analysis of the neural oscillators. Figure 2 compares the eigenvalue analyses of the theoretically derived ΔC and numerical simulation. The theoretically derived eigenfunctions with the maximal and minimal eigenvalues (E1 and E100) are consistent with the numerically simulated eigenfunctions (Fig. 2 (A2) and (B2)). The theoretical result also matches the numerical results for the eigenfunctions with second maximal and minimal eigenvalues (E2 and E99) (data not shown). These results suggest that our theory can identify the neural feature space of neurons firing periodically if we know only the PRC.

When applying the theory to extracting the feature space of real neurons, we have to use the PRCs estimated from a finite sample of noisy phase responses measured in vitro. Here, we verified how estimation errors of the PRCs affect the reliability of the STCs. We numerically generated artificial noisy phase response data using
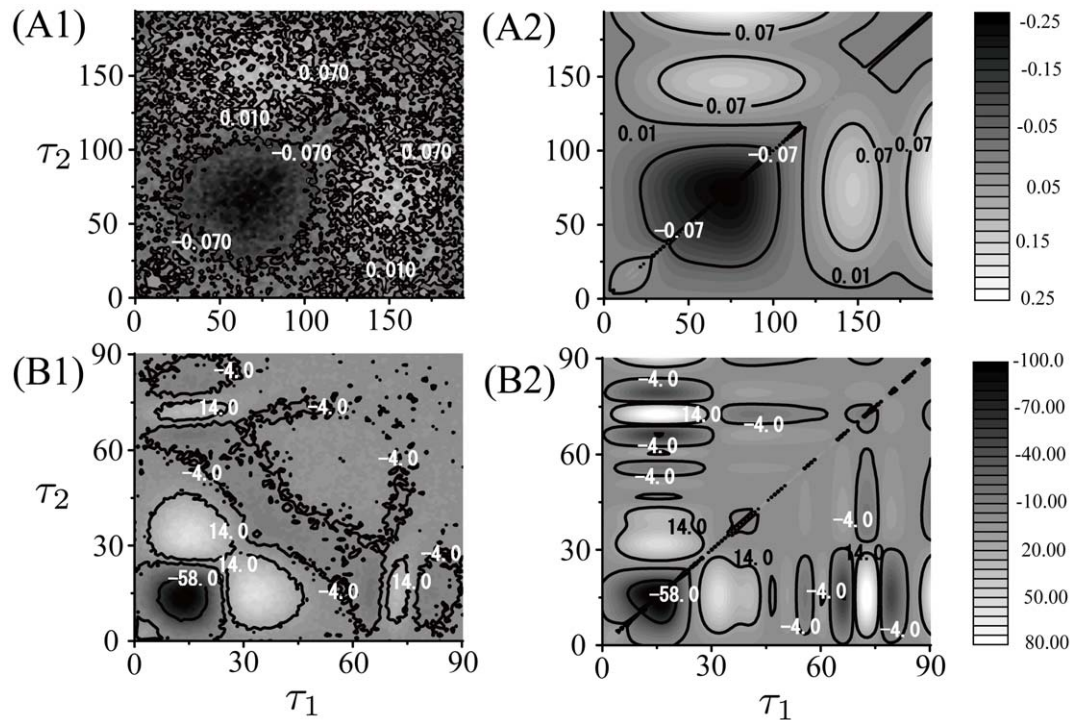

Figure 1. Numerically simulated STC (A1, B1) and theoretically derived STC (A2, B2). Here the delta-peak at the point $\tau_1 = \tau_2$ is replaced with the average of the nearest matrix elements values. (A) Type I ML model, $\sigma = 1.0\ (\mu A)$. (B) Type II ML model, $\sigma = 6.0\ (\mu A)$. The DC input current used in (A) and (B) is 41.0 (μA) and 95.0 (μA) respectively, which induces regular spikes with intervals of about 195.83 msec and 91.17 msec. In all the experiments, the numerically simulated STC were computed using a sample of 10^9 spikes and the matrix size of the STC was 100×100.
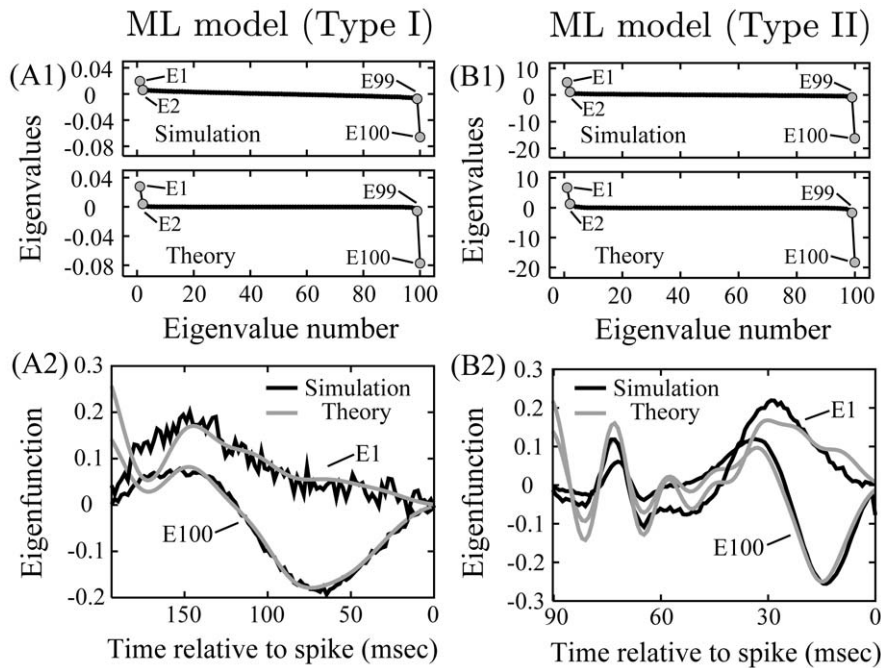doi:10.1371/journal.pone.0050232.g001

Figure 2. Eigenvalue analyses of the theoretically derived ΔC and numerical simulation. (A1, B1) The eigenvalue spectrum of the numerically simulated ΔC (upper) and the eigenvalue spectrum of the theoretically obtained ΔC (bottom). (A2, B2) The eigenfunctions associated with the maximal eigenvalue (E1) and minimal eigenvalues (E100). The eigenfunctions derived from the theoretically obtained ΔC (gray line) mostly match those derived from the numerically simulated ΔC (black line). This eigenvalue analysis is independent of the matrix size of ΔC.
doi:10.1371/journal.pone.0050232.g002

the Type I ML model, and we estimated the PRC from the artificial data with the maximum a posteriori (MAP) estimation algorithm that we previously proposed [29]. After that, we compared the STC, the eigenvalue spectra and the eigenfunctions calculated from the estimated PRC with those from the PRC derived with the adjoint method (Fig. 1(A2) and Figs. 3(B)-(D)). As shown in Fig. 3(A), the estimated PRC with finite noisy samples conforms to the PRC derived with the adjoint method in the first half of the period, but is different in the second half of the period. As shown in Figs. 1(A2), 3(B) and 3(D), the STC and the eigenfunctions calculated with the estimated PRC are in good agreement with ones derived by the adjoint method at earlier times relative to the spike, but they have few differences at later times relative to the spike.

Feature Space of the Hippocampal CA1 Pyramidal Neurons

We identified the feature space of rat hippocampal CA1 pyramidal neurons oscillating in the theta frequency range (4–14 Hz) [15–17]. Figure 4 (A) shows the PRCs of pyramidal neurons, which have been measured in vitro in previous works [18,30,31].

Figure 4 (B) shows the STCs calculated from the PRCs and Fig. 4 (C) the eigenvalue spectra for the STCs arranged in order of absolute magnitude. Note that it was impossible to accurately distinguish between a zero and nonzero eigenvalue because of the numerical precision limitation. Instead, we evaluated the cumulative contribution ratio of the magnitude of the eigenvalues (Fig. 4 (D)). Figure 4 (E) shows the top 4 eigenfunctions highly contributing to the representation of the feature spaces for each neuron. Those phasic relationships to the neuron firing (i.e., positive and negative parts of the eigenfunctions) are different from each other. Here, to elucidate the common characteristics of those

eigenfunctions representing highly sensitive inputs of those neurons, we calculated power spectra of the eigenfunctions (Fig. 4(F)).

Here we checked a total of five samples including two other samples of pyramidal neurons not shown in Fig. 4. E1 in all five samples, including the three samples in Fig. 4, has negative eigenvalues, and the power spectra of E1 in all samples except for neuron 2 have peaks in the theta frequency range. For neuron 2, the power spectrum of E1 has a peak at zero frequency and is relatively large in the theta frequency range. On the other hand, E2 in all samples except for neuron 1 has positive eigenvalues, and the power spectra of E2 in all of five samples have the first peaks at zero frequency and second peaks in the gamma frequency range (20–80 Hz). Therefore, we can conclude that the first principal component of the feature space is the suppressive eigenfunction mainly composed of theta frequency components, whereas the second principal component is the excitatory eigenfunction mainly composed of DC and gamma frequency components. This result suggests that theta waves suppress neural activity, leading to longer ISIs than the average period T, whereas DC and gamma waves enhance neural activity, leading to shorter ISIs.

Discussion

In this study, we proposed the general formulation to relate the PRC and the nth moment of the STE. At first, using the new formulation, we analytically derived approximate equations that relate the PRC to the STA. The relational equation between the STA and PRC was equal to the equation derived by Ermentrout et al. [13]. Thus, our formulation method includes their theory. Next, using the formulation, we were able to successfully derive the relational equation between the PRC and the STC. This relational equation allows us to determine the feature space only from the PRC.
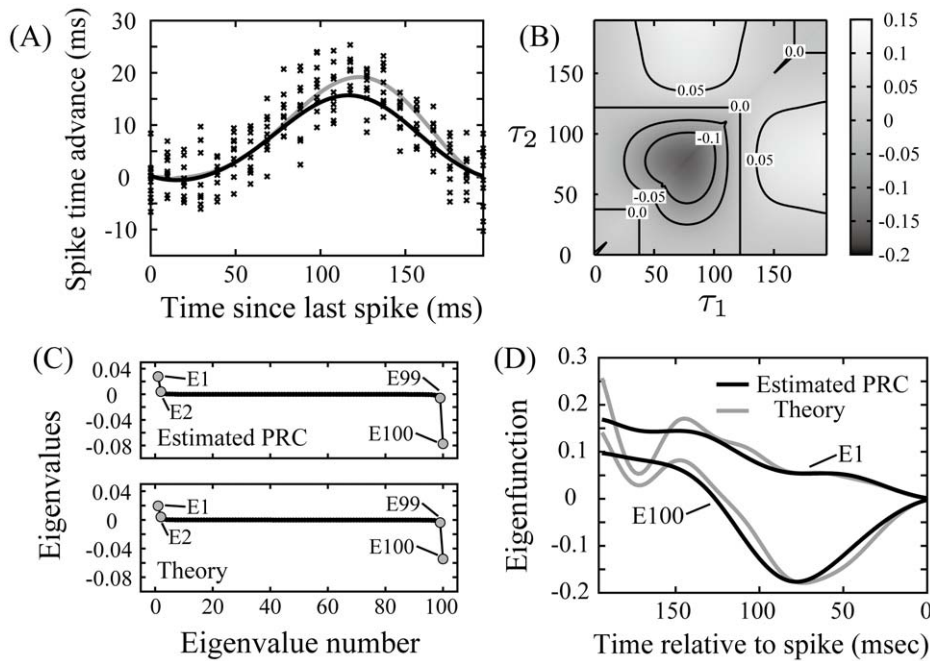
Figure 3. The STC, the eigenvalue spectrum and the eigenfunctions calculated with the PRC estimated from a finite number of artificial noisy data. (A) Crosses show artificial phase response data generated with the Type I ML model. $\gamma = 0.45$, $L = 20$ and $N = 10$. The gray solid line is the PRC derived with the adjoint method, and the black solid line indicates an estimated PRC as a result of applying the MAP estimation algorithm to the artificial data. (B) STC calculated from the estimated PRC with the artificial data. $\sigma = 1.0$. (C) Upper: the eigenvalue spectrum of ΔC calculated from the estimated PRC with finite noisy samples. Lower: one calculated from the PRC derived with the adjoint method, which is the same as the lower part of Fig. 2(A1). (D) The eigenfunctions associated with the maximum and the minimal eigenvalues, E1 and E100. Black solid lines are calculated with the estimated PRC. Gray solid lines are calculated with the PRC with the adjoint method, which are the same as the gray solid lines of Fig. 2(A2).

doi:10.1371/journal.pone.0050232.g003

We used the relational equation to identify the feature space of the rat hippocampal CA1 pyramidal neurons oscillating in the theta frequency range. We showed that the first principal component representing the feature space is the suppressive eigenfunction mainly composed of theta frequency components, whereas the second principal component is the excitatory eigenfunction mainly composed of DC and gamma frequency components. This result suggests that the hippocampal CA1 pyramidal neurons oscillating in the theta frequency range are commonly sensitive to inputs composed of DC, theta, and gamma frequency components. Theta waves prolong the ISIs of theta oscillating neurons whereas DC and gamma waves shorten them. Note that the DC sensitivity is trivial because an increase in the depolarization current shortens the ISIs. Therefore, our results imply that during theta oscillation the ISIs of the CA1 pyramidal neurons can be modulated by inputs oscillating at theta and gamma frequencies. Several studies have observed the theta oscillation in the CA1 area of the hippocampus in freely behaving rats and have found that the gamma waves are superimposed on the theta oscillation [34], and many researchers have focused on interactions between theta and gamma oscillations in an attempt to account for the temporal coding of the hippocampus [35]. Our finding suggests that interactions between theta and gamma oscillations can be realized at the single neuron level.

The shape of PRCs shown in Fig. 4 is different from those measured by Netoff et al [36]. This is because the periods of oscillatory activates we tuned in measuring PRCs are slightly shorter than 100 ms intervals they used. It is well known that the shape of PRCs strongly depends on the period of the oscillation [37].

As expressed in Eqs. (7) and (8), we ignored the refractoriness in the formulation for the moment of STE. Using Omori et al.'s formulation [12], we can deal with the refractory effect, because this formulation enables us to prevent miscounting events in which the spike is reset after a spike to just prior to a spike.

Small excitatory inputs applied at the end of the phase cannot advance the action potential to a time prior to the application of the stimulus. This causality limit changes the noise characteristics of a measured PRC at the end of the phase even when no dynamical change may occur. However, the LPE we used to describe stochastic fluctuations of phase responses in the MAP estimation algorithm does not have a resetting mechanism immediately after spike generation as in the integrate-and-fire neuron model, so this algorithm cannot deal with the causality limit problem [18,29,30]. One approach to account for this effect to estimate the phase advance where the mean is estimated using a truncated Gaussian distribution to describe stochastic fluctuations of phase responses [38].

We obtained the STC shown in Figs. 1 (A1) and (B1) from lots of spikes. The number of neural spikes required for a stable calculation of the STC is nearly the square of the number required for the STA. Ermentrout et al. calculated the STA of the olfactory bulb mitral cell from several thousand spikes [13]; therefore, the STC requires more than 10^6 spikes, which is much more than what would be available in a physiological experiment. On the other hand, the PRCs have been measured from just several hundred spikes in several real neurons [18,39–43]. Equation (15) enables us to obtain the STC of the real neuron through the PRC.

The PRCs of the hippocampal CA1 pyramidal neurons recorded in vitro used here are defined as changes in ISI between
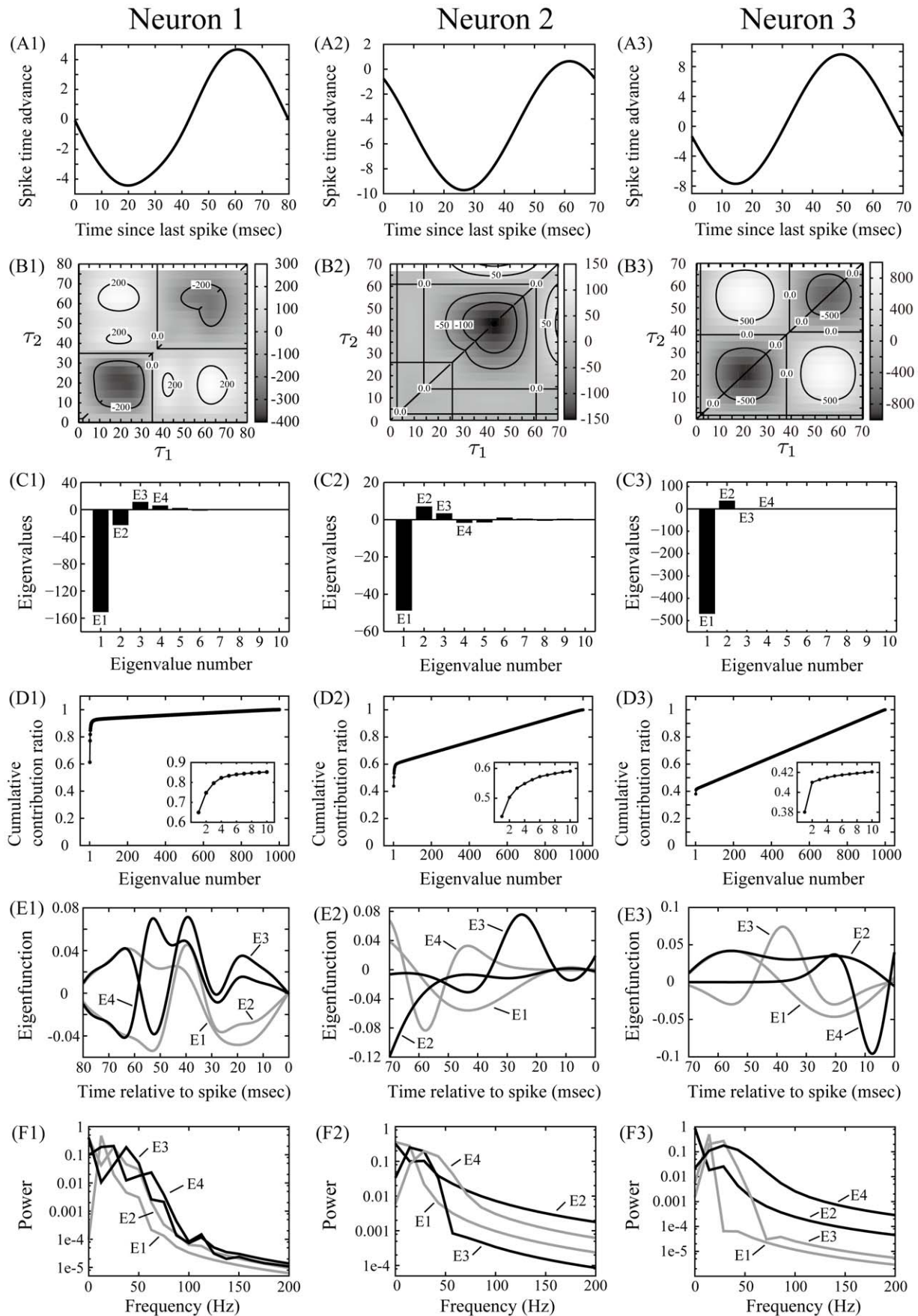
Figure 4. PRCs, STCs and eigenvalue analysis results for 3 rat hippocampal CA1 pyramidal neurons. (A) PRCs of 3 rat hippocampal CA1 pyramidal neurons [18]. The firing period is (A1) 80 msec and (A2, A3) 70 msec. (B) The STCs for PRCs shown in (A). It is calculated using Eq. (15) into which we substitute the estimated PRC and noise intensity. The matrix size is 1000×1000. (C) The eigenvalue spectra of ΔC arranged in order of absolute magnitude. Unlike Fig. 2, the number on the eigenvalues in Fig. 3 is assigned in order of absolute magnitude. (D) The cumulative contribution ratio of the magnitude of the eigenvalues. (E) The eigenfunctions for eigenvalues E1, E2, E3 and E4. (F) The power spectra of the top 4 eigenfunctions shown in (E).
doi:10.1371/journal.pone.0050232.g004

two successive single spikes in response to small perturbations for regularly firing neurons. However, temporal spike patterns of the hippocampal CA1 pyramidal neurons in vivo show more bursty behaviors than those we assume here. Hence, our assumption does not correspond to actual behaviors very well. Despite this, our theory can be straightforwardly applied to bursty situations. For bursty neurons, the burst phase response curves (BPRCs), which are defined as changes in the interval between two successive bursts in response to small perturbations, can be obtained by computing with an infinitesimal perturbation approximation and by directly stimulating the neurons, as we did [44–46]. By using BPRCs instead of PRCs, one can expect to capture coding properties closer to those of in vivo situations.

To make in vitro experiments for measuring the PRC look like in vivo as much as possible, Lengyel et al. injected sinusoidal inhibitory conductance with the dynamic clamp, which mimics hippocampal theta oscillation, into somata of CA3 pyramidal neurons [40]. In contrast, we injected DC depolarizing currents into somata of CA1 pyramidal neurons to evoke periodic firing. By using the PRCs under external periodic perturbation, one can expect to capture coding properties closer to those of in vivo situations.

As described in Methods section, depending on bifurcation structures, neural oscillators can be classified as Type I and Type II [47]. It has been proved that near a bifurcation point, the infinitesimal PRC of Type I neuron only has positive values, whereas the infinitesimal PRC of Type II neuron has positive and negative (biphasic) values [33]. Thus, purely positive PRCs are habitually called Type I PRCs, whereas biphasic PRCs are called Type II PRCs. In line with this argument, Steifiel et al. showed physiologically and numerically that cholinergic action, which causes the down-regulation of slow voltage-dependent potassium currents such as the M-current, could switch the PRC from Type II to Type I [48,49]. This result suggests that cholinergic modulation may change the bifurcation structure of neural dynamics, resulting in a qualitative switch of the PRCs type. If this suggestion is true, cholinergic modulation may cause a change in the feature space of neurons reflected in a qualitative switch of the PRCs type as shown in Figs. 1 and 2. From the results of Stiefel et al and our theory, there arises a possibility that we can do a longitudinal study of a neural system from the molecular level to the computational level.

Author Contributions

Conceived and designed the experiments: KO TA. Performed the experiments: KO. Analyzed the data: KO. Contributed reagents/materials/analysis tools: HM. Wrote the paper: KO TO MO TA.

References

1. Marmarelis PZ, Naka K (1972) White-noise analysis of a neuron chain: an application of the wiener theory. Science 175: 1276–1278.
2. Schwartz O, Pillow JW, Rust NC, Simoncelli EP (2006) Spike-triggered neural characterization. J Vision 6: 484–507.
3. Pillow JW, Simoncelli EP (2006) Dimensionality reduction in neural models: An information-theoretic generalization of spike-triggered average and covariance analysis. J Vision 6: 414–428.
4. Rust NC, Schwartz O, Movshon JA, Simoncelli EP (2004) Spike-triggered characterization of ex-citatory and suppressive stimulus dimensions in monkey V1. Neurocomputing 58–60: 793–799.
5. Ohzawa I, DeAngelis GC, Freeman RD (1997) The neural coding of stereoscopic depth. NeuroRe-prot 8: 3–12.
6. Dayan P, Abbott LF (2001) Theoretical Neuroscience: Computational and Mathematical Modeling of Neural Systems, MIT Press, chapter 1–4. 1st edition.
7. Simoncelli EP, Paninski L, Pillow J, Schwartz O (2004) The Cognitive Neurosciences, MIT Press, chapter 23 Characterization of Neural Responses with Stochastic Stimuli. 3rd edition, 327–338.
8. Rust NC, Schwartz O, Movshon JA, Simoncelli EP (2005) Spatiotemporal elements of macaque v1 receptive fields. Neuron 46: 945–956.
9. Paninski L (2006) The spike-triggered average of the integrate-and-fire cell driven by gaussian white noise. Neural Comp 18: 2592–2616.
10. Arcas BA, Fairhall AL, Bialek W (2003) Computation in a single neuron: Hodgkin and huxley revisited. Neural Comp 15: 1715–1749.
11. Arcas BA, Fairhall AL (2003) What causes a neuron to spike? Neural Comp 15: 1789–1807.
12. Omori T, Aonishi T, Okada M (2010) Switch of encoding characteristics in single neurons by subthreshold and suprathreshold stimuli. Phys Rev E 81: 021901.
13. Ermentrout GB, Galan RF, Urban NN (2007) Relating neural dynamics to neural coding. Phys Rev Lett 99: 248103.
14. Hong S, Arcas BA, Fairhall AL (2007) Single neuron computation: From dynamical system to feature detector. Neural Comp 19: 3133–3172.
15. Klausberger T, Somogyi P (2008) Neuronal diversity and temporal dynamics: the unity of hip-pocampal circuit operations. Science 321: 53–57.
16. Fellous JM, Sejnowski TJ (2000) Cholinergic induction of oscillations in the hippocampal slice in the slow (0.5–2 hz), theta (5–12 hz), and gamma (35–70 hz) bands. Hippocampus 10: 187–197.
17. DeCoteau WE, Thorn C, Gibson DJ, Courtemanche R, Mitra P, et al. (2007) Learning-related coordination of striatal and hippocampal theta rhythms during acquisition of a procedural maze task. Proc Natl Acad Sci U S A 104: 5644–56491.
18. Ota K, Omori T, Watanabe S, Miyakawa H, Okada M, et al. (2011) Measurement of infinitesimal phase response curves from noisy real neurons. Phys Rev E 84: 041902.
19. Draguhn A, Traub RD, Schmitz D, Jefferys JGR (19980) Electrical coupling underlies high-frequency oscillations in the hippocampus in vitro. Nature 394: 189–192.
20. Traub RD, Whittington MA, Colling SB, Buzsaki G, Jefferys JGR (1996) Analysis of gamma rhythms in the rat hippocampus in vitro and in vivo. J Physiol 493.2: 471–484.
21. Kuramoto Y (1984) Chemical oscillations, waves and turbulence. Springer–Verlag.
22. Kawamura Y, Nakao H, Arai K, Kori H, Kuramoto Y (2008) Collective phase sensitivity. Phys Rev Lett 101: 024101.
23. Teramae J, Fukai T (2008) Temporal precision of spike response to uctuating input in pulse-coupled networks of oscillating neurons. Phys Rev Lett 101: 248105.
24. Nakao H, Arai K, Kawamura Y (2007) Noise-induced synchronization and clustering in ensembles of uncoupled limit-cycle oscillators. Phys Rev Lett 98: 184101.
25. Tsubo Y, Teramae JN, Fukai T (2007) Synchronization of excitatory neurons with strongly het-erogeneous phase responses. Phys Rev Lett 99: 228101.
26. Ermentrout GB, Beverlin II B, Troyer T, Netoff TI (2011) The variance of phase-resetting curves. J Comput Neurosci 31: 185–97.
27. Risken H (1996) The Fokker-Planck Equation: Methods of Solution and Applications. Springer.
28. Mato G, Samengo I (2008) Type I and type II neuron models are selectively driven by differential stimulus features. Neural Comp 20: 2418–2440.
29. Ota K, Omori T, Aonishi T (2009) Map estimation algorithm for phase response curves based on analysis of the observation process. J Comput Neurosci 26: 185–202.
30. Ota K, Aonishi T (2012) Phase Response Curves in Neuroscience: Theory, Experiment,and Analysis, Springer, chapter 8 Bayesian Approach to Estimating Phase Response Curves. 1st edition, 179–203.
31. Ota K, Tsunoda T, Omori T,Watanabe S, Miyakawa H, et al. (2009) Is the langevin phase equation an efficient model for oscillating neurons? J Phys Conf Ser 197: 012016.

　　　　　　　　　　　　　　9

32. Morris C, Lecar H (1981) Voltage oscillations in the barnacle giant muscle _ber. Biophys J 35: 193–213.

33. Ermentrout GB (1996) Type I membranes, phase resetting curves, and synchrony. Neural computation 8: 979–1001.

34. Buzsaki G (2002) Theta oscillations in the hippocampus. Neuron 33: 325–340.

35. Lisman J (2005) The theta/gamma discrete phase code occuring during the hippocampal phase precession may be a more general brain coding scheme. Hippocampus 15: 913–922.

36. Netoff T, Schwemmer MA, Lewis TJ (2012) Phase Response Curves in Neuroscience: Theory, Experiment,and Analysis, Springer, chapter 5 Experimentally Estimating Phase Response Curves of Neurons: Theoretical and Practical Issues. 1st edition, 95–129.

37. Fink CG, Booth V, Zochowski M (2012) Phase Response Curves in Neuroscience: Theory, Experiment,and Analysis, Springer, chapter 19 Effects of the Frequency Dependence of Phase Response Curves on Network Synchronization. 1st edition, 475–487.

38. Polhamus DG, Wilson CJ, Paladini CA (2012) Phase Response Curves in Neuroscience: Theory, Experiment,and Analysis, Springer, chapter 7 PRC Estimation with Varying Width Intervals. 1st edition, 163–177.

39. Galan RF, Ermentrout GB, Urban NN (2005) Efficient estimation of phase-resetting curves in real neurons and its significance for neural-network modeling. Phys Rev Lett 94: 158101.

40. Lengyel M, Kwag J, Paulsen O, Dayan P (2005) Matching storage and recall: hippocampal spike timing-dependent plasticity and phase response curves. Nature Neurosci 8: 1677–1683.

41. Tsubo Y, Takada M, Reyes AD, Fukai T (2007) Layer and frequency dependencies of phase response properties of pyramidal neurons in rat motor cortex. European Journal of Neuroscience 25: 3429.

42. Netoff TI, Banks MI, Dorval AD, Acker CD, Haas JS, et al. (2005) Synchronization in hybrid neuronal networks of the hippocampal formation. J Neurophys 93: 1197–1208.

43. Tateno T, Robinson HP (2007) Phase resetting curves and oscillatory stability in interneurons of rat somatosensory cortex. Biophys 92: 683.

44. Aoyagi T, Takekawa T, Fukai T (2003) Gamma rhythmic bursts: Coherence control in networks of cortical pyramidal neurons. Neural Comp 15: 1035–1061.

45. Takekawa T, Aoyagi T, Fukai T (2007) Synchronous and asynchronous bursting states: role of intrinsic neural dynamics. J Comput Neurosci 23: 189–200.

46. Sherwood WE, Guckenheimer J (2010) Dissecting the phase response of a model bursting neuron. SIAM J Appl Dyn Sys 9(3): 659–703.

47. Rinzel JR, Ermentrout GB (1998) Methods in Neuronal Modeling: From Ions to Networks, MIT Press, chapter Analysis of neural excitability and oscillations, in Methods in Neuronal Modeling.

48. Stiefel KM, Gutkin BS, Sejnowski TJ (2008) Cholinergic neuromodulation changes phase response curve shape and type in cortical pyramidal neurons. PLoS ONE 3: e3947.

49. Stiefel KM, Gutkin BS, Sejnowski TJ (2009) The effects of cholinergic neuromodulation on neuronal phase-response curves of modeled cortical neurons. J Comput Neurosci 26: 289–301.